CERN - European Organization for Nuclear Research

LCD-Note-2009-002

A Luminosity Calorimeter for CLIC

H. Abramowicz, R. Ingbir, S. Kananov, A. Levy, I. Sadeh*

* *School of Physics and Astronomy, The Raymond and Beverly Sackler Faculty of Exact Sciences, Tel Aviv University, Tel Aviv, Israel.*

November 2009

Abstract

For the relative precision of the luminosity measurement at CLIC, a preliminary target value of 1% is being assumed. This may be accomplished by constructing a finely granulated calorimeter, which will measure Bhabha scattering at small angles. In order to achieve the design goal, the geometrical parameters of the calorimeter need to be defined. Several factors influence the design of the calorimeter; chief among these is the need to minimize the error on the luminosity measurement while avoiding the intense beam background at small angles. In this study the geometrical parameters are optimized for the best performance of the calorimeter. In addition, the suppression of physics background to Bhabha scattering is investigated and a set of selection cuts is introduced.

Presented at: *FCAL Collaboration Meeting, Zeuthen, June 2009*

1 Introduction

The focus of this study is the luminosity calorimeter (LumiCal) of the Compact Linear Collider (CLIC). Bhabha scattering will be used as the gauge process for the luminosity measurement at CLIC. This is motivated by the fact that the cross-section of Bhabha scattering is large and dominated by electromagnetic processes, and thus can be calculated with very high precision [1, 2, 3, 4, 5].

Several studies have been done of the luminosity calorimeter at the International Linear Collider (ILC) [6, 7]. The main differences in the luminosity measurement between the ILC and CLIC is the center-of-mass energy; while for the ILC it is 500 GeV (upgradable to 1 TeV), for CLIC it is expected to go up to 3 TeV [8]. This has repercussions both on the cross-section of Bhabha scattering, which decreases with energy, and on the cross-section of the physics background to Bhabha scattering, which goes up with energy. In addition, the beam induced background at CLIC is more severe, due to the increase in beam energy as well as to differences in other bunch parameters. The baseline configuration of the calorimeter presented here is similar to the LumiCal of the ILC, but it takes into account the change in the beam conditions. Accordingly, many references to ILC studies are given.

The requirement for LumiCal is to enable a measurement of the integrated luminosity with a relative precision smaller than 1 % [8]. It will be shown here that in order to perform this measurement, the polar angle of incident showers must be measured with high precision. This may be done by demanding fine granulation in the radial direction. Another important factor is the percentage of the Bhabha cross-section which is accessible to the measurement. The cross-section drops quickly with the polar angle, and so the minimal polar angle in the acceptance range of LumiCal must be low in order to ensure high statistics. On the other hand, the inner radius of LumiCal should not be set to a too-low value, since at small polar angles the beam background is intense. If this background is high, damage to the sensors of LumiCal as well as backscattering from the front of LumiCal become a problem.

In the following study a proposal for the design of LumiCal for CLIC is presented. In Sect. 2 the chosen design parameters are presented. The intrinsic properties of LumiCal are then defined and given a quantitative measure. The optimization of these parameters is shown in Sect. 3. The impact of the beam structure on the design of LumiCal is discussed as well. The results are presented in most cases for two center-of-mass energies, 500 GeV and 3 TeV, as these represent respectively the lowest and highest beam energies expected for CLIC. Section 4 addresses the suppression of physics background to Bhabha scattering. We conclude with a short summary, given in Sect. 5.

Luminosity Measurement at CLIC

The measured luminosity is defined as

$$\mathcal{L} = \frac{N_{\mathrm{B}}}{\sigma_{\mathrm{B}}}, \tag{1}$$

where N_{B} stands for the counted number of Bhabha events in a well-defined polar angular range and σ_{B} is the integrated Bhabha cross-section in this range.

Several factors, such as the energy resolution and the bias in the reconstruction of the position of showers, induce an uncertainty in the luminosity measurement [7, 9]. The uncertainty manifests itself as miss-counting of the number of expected Bhabha scattering events within the fiducial volume (acceptance range). It is convenient to define the relative bias in counting as

$$\delta\mathcal{N} \equiv \frac{N_{gen} - N_{rec}}{N_{gen}}\Bigg|_{\theta^f_{min}}^{\theta^f_{max}}, \tag{2}$$

where N_{rec} and N_{gen} are respectively the number of reconstructed and generated Bhabha events, and θ^f_{min} and θ^f_{max} are the respective low and high bounds on the fiducial volume of LumiCal. Accordingly, the relative uncertainty on the integrated luminosity can be expressed as

$$\frac{\Delta\mathcal{L}}{\mathcal{L}} = \delta\mathcal{N}. \tag{3}$$

Simulation Tools

Detector simulation - The response of LumiCal to the passage of particles was simulated using MOKKA, version 06-05-p02 [10]. MOKKA is an application of a general purpose detector simulation package, GEANT4, of which version 9.0.p01 was used [11]. The GEANT4 range-cut parameter was set to 0.005 mm. The MOKKA model chosen was LDC00_03Rp, where LumiCal is constructed by the LumiCalX super driver. The output of MOKKA is in the LCIO format, which may be processed by MARLIN, a C++ software framework for the ILC software [12]. Version 00-09-08 of MARLIN was used.

Event generators - The spectrum of the incoherent pairs presented in Sect. 3.4 was generated using GUINEA-PIG [13], an e^+e^- beam-beam simulation program. For the present work, realistic (non-gaussian) particle distributions of the CLIC 3 TeV beams have been used [14]. In Sect. 4 a physics sample consisting of Bhabha scattering events is used. The events were generated using BHWIDE [15]. BHWIDE is a wide-angle Bhabha Monte Carlo (MC), which contains the electroweak contributions, which are important for the high energy e^+e^- interactions considered here. The background to Bhabha scattering was simulated using WHIZARD, a program system designed for the efficient calculation of multi-particle scattering cross-sections and simulated event samples [16, 17, 18]. For the current study the luminosity spectrum, due to the emission of beamstrahlung radiation, was not taken into account when generating the BHWIDE and the WHIZARD event samples. The nominal center-of-mass energy was used instead.

2 Intrinsic Parameters

LumiCal is a tungsten-silicon sandwich calorimeter. The front face of LumiCal is placed 2.27 m from the interaction point (IP). LumiCal is placed on the outgoing beam axis and is tilted to be perpendicular to the outgoing beam. The LumiCal inner radius is 10 cm, and its outer radius is 35 cm, resulting in a polar angular coverage of 44 to 153 mrad. The calorimeter consists of 40 layers. Each layer is made up of 3.5 mm thick tungsten, which is equivalent to 1 radiation length (defined below). Behind each tungsten layer there is a 0.6 mm ceramic support, a 0.3 mm silicon sensor plane, and a 0.1 mm gap for electronics. The transverse plane is subdivided in the radial and azimuthal directions. The number of radial divisions is 50, and the number of azimuthal divisions is 48. Figure 1 presents the segmentation scheme of a LumiCal sensor half plane. The current simulation of the detector does not include "realistic" features of the calorimeter, such as dead material at the inner and outer radii of LumiCal, or gaps between sensor tiles. These and other details will be added to the MOKKA simulation in the future, and their affect on the performance of LumiCal will be studied.

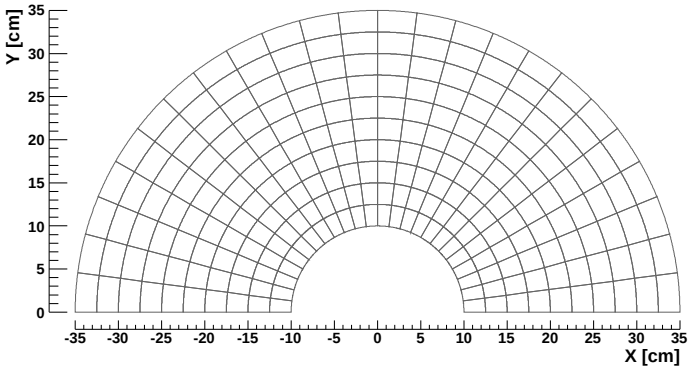

Figure 1: Half plane of LumiCal silicon sensors. In this schematic drawing only every fifth radial segment is drawn.

The design parameters presented here have been determined such that the performance of LumiCal is optimized. The considerations which were taken into account in the optimization process are discussed in Sect. 3. In the following, several parameters which quantify the performance of LumiCal are defined and their values for the current geometry are determined.

2.1 Development of Electromagnetic Showers

When a high-energy electron or photon is incident on a thick absorber, it initiates an electromagnetic (EM) shower as pair production and bremsstrahlung generate more electrons and photons with lower energy. The characteristic amount of matter traversed for these related interactions is

called the *radiation length*, X_0. It is both the mean distance over which a high-energy electron looses all but $1/e$ of its energy by bremsstrahlung, and $\frac{7}{9}$ of the mean free path for pair production by a high-energy photon [19]. The radiation length is also the appropriate scale length for describing high-energy electromagnetic showers. Electron energies eventually fall below the critical energy (defined below), and then dissipate their energy by ionization and excitation, rather than by the generation of more shower particles.

The transverse development of electromagnetic showers scales fairly accurately with the Molière radius, $R_{\mathcal{M}}$, given by [19]

$$R_{\mathcal{M}} = X_0 \frac{E_s}{E_c}, \tag{4}$$

where $E_s \approx 21$ MeV, and E_c is the *critical energy*, which is defined as the energy at which the ionization loss per radiation length is equal to the electron energy. On average, only 10% of the energy of an EM shower lies outside a cylinder with radius $R_{\mathcal{M}}$ around the shower-center.

Figure 2a shows the distribution of the distance around the shower-center, in which 90 % of the integrated shower energy may be found, using 250 GeV and 1.5 TeV electron showers. The two distributions peak around 15 mm, demonstrating that the Molière radius does not depend strongly on the shower energy. Figure 2b shows the shower profiles of a 250 GeV and of a 1.5 TeV electron shower. The 1.5 TeV shower is larger in the transverse direction, but most of the energy deposits at large distance from the center of the shower are of low energy. This can be deduced from the fact that on average 90 % of the energy is within 15 mm of the shower-center.

2.2 Energy Resolution

LumiCal is designed in such a way that incident high energy electrons and photons deposit practically all of their energy in the detector. Prevention of leakage through the edges of LumiCal is possible by defining fiducial cuts on the minimal and maximal reconstructed polar angles of the particle showering in LumiCal, θ_{min} and θ_{max}. In order to achieve stable energy resolution in LumiCal, showers must be well-contained. The relative energy resolution, σ_E/E, is usually parametrized as

$$\frac{\sigma_E}{E} = \frac{a_{res}}{\sqrt{E_{beam}}}, \tag{5}$$

where E and σ_E are, respectively, the most probable value, and the root-mean-square of the signal distribution for a beam of electrons. The energy of the electron beam, E_{beam}, is given in units of GeV. In the following, we shall refer to the parameter a_{res} as the energy resolution of LumiCal.

Figure 3a shows the energy resolution as a function of θ_{min} for electron showers with energy, $E_{sh} = 1.5$ TeV. The maximal polar angle is kept constant. Stable energy resolution is achieved for

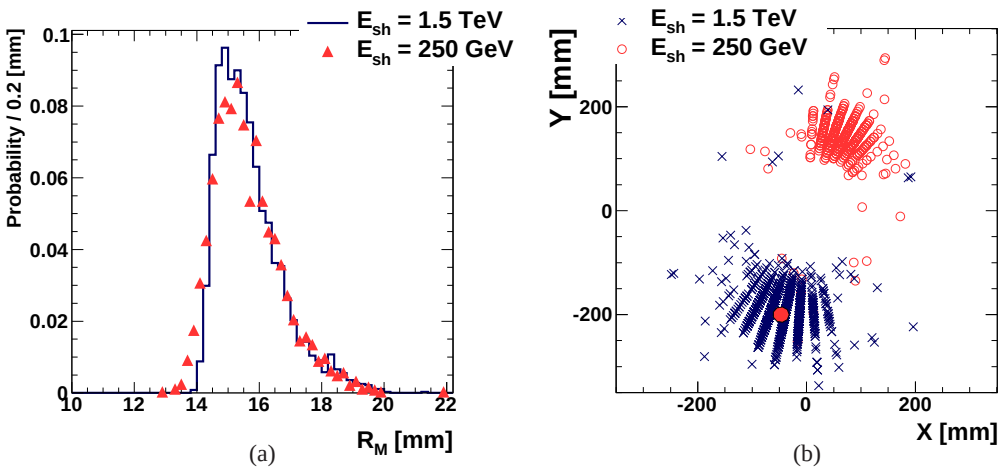

Figure 2: (a) Normalized distribution of the distance around the shower-center, in which 90 % of the integrated shower energy may be found, using 250 GeV and 1.5 TeV electron showers, as indicated in the figure. (b) Scatter plot of the energy deposits in LumiCal in the xy-plane, integrated over all layers. Two showers are shown, with energies $E_{sh} =$ 250 GeV and 1.5 TeV, as indicated in the figure. The full circle marks an area bound within one Molière radius around the center of the 1.5 TeV shower, which is at $\{X,Y\} = \{-47,-200\}$ mm in this example.

θ_{min} = 50 mrad. A similar evaluation was done for a constant θ_{min} and a changing θ_{max}, resulting in an optimal cut at θ_{max} = 130 mrad, as shown in Fig. 3b. The size of showers does not depend strongly on energy down to $E_{sh} = 250$ GeV (Fig. 2a). The same polar bounds therefore stabilize the energy resolution for showers with lower energy as well. The error bars are derived from the error on the fits of the value of σ_E, from which a_{res} was extracted.

The fiducial volume of LumiCal for $250 < E_{sh} < 1500$ GeV is thus defined to be the polar angular range

$$50 < \theta^f < 130 \text{ mrad}. \tag{6}$$

The dependence of the energy resolution on the energy of the electron which initiated the shower, E_{sh}, is shown in Fig. 4. Only electron showers from particles which were inside the fiducial volume of LumiCal were taken into account. The energy resolution is, therefore, $a_{res} = 0.21 \pm 0.02\ \sqrt{\text{GeV}}$.

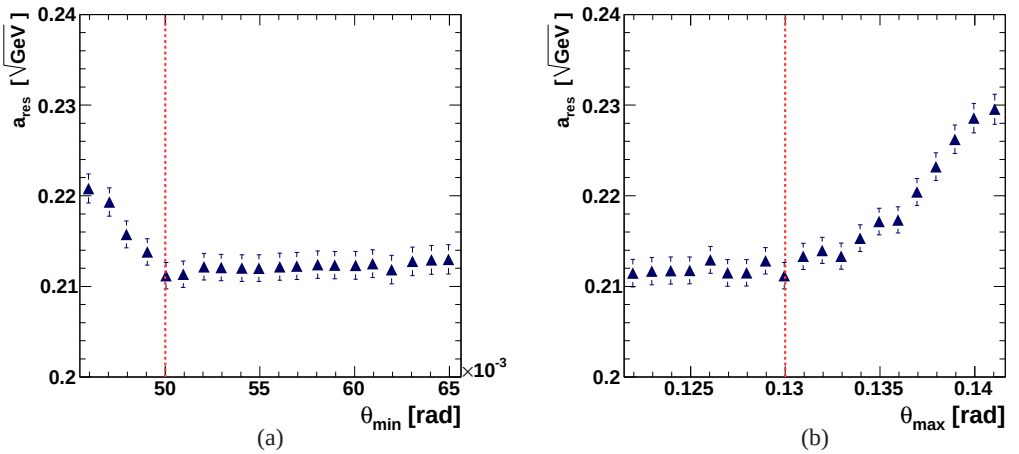

(a) (b)

Figure 3: The energy resolution, a_{res}, for 1.5 TeV electrons as a function of the minimal polar angle, θ_{min}, (a) and as a function of the maximal polar angle, θ_{max}, (b). The dashed lines mark the fiducial volume of LumiCal at $\theta^f_{min} = 50$ and $\theta^f_{max} = 130$ mrad.

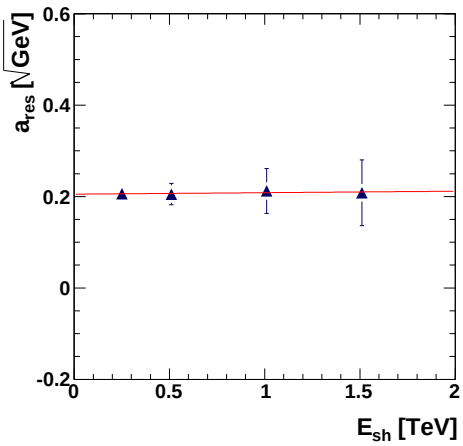

Figure 4: Dependence of the energy resolution, a_{res}, on the energy of an electron shower, E_{sh}.

2.3 Calibration of the detector Signal

In order to determine the energy of showering particles in LumiCal, it is necessary to know the relation between this energy and the integrated deposited energy in the detector (measured signal). A calibration curve which demonstrates this relation is shown in Fig. 5. The signal is linear within the range of energies which is presented.

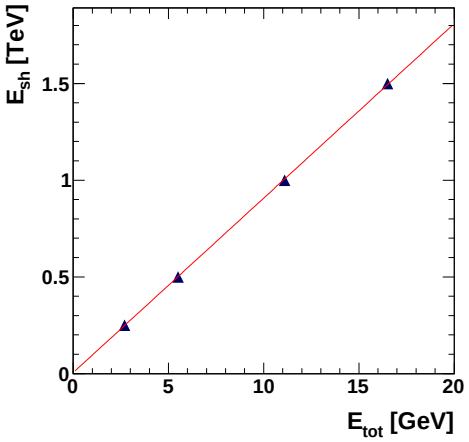

Figure 5: Calibration curve between the energy of a shower in LumiCal, E_{sh}, and the integrated deposited energy in LumiCal, E_{tot}.

2.4 Reconstruction of the Polar Angle

The polar angle of an EM shower in LumiCal is reconstructed by averaging over the individual cells in the detector in which energy was deposited. This is done for cell i using the polar angle of the center of the cell, θ_i, and a weight function, $\mathcal{W}_i$, such that

$$< \theta >= \frac{\sum_i \theta_i \cdot \mathcal{W}_i}{\sum_i \mathcal{W}_i}. \tag{7}$$

Weights are determined by the so-called logarithmic weighting [20], for which

$$\mathcal{W}_i = \max\{\ 0\ ,\ \mathcal{C} + \ln\frac{E_i}{E_{tot}}\}, \tag{8}$$

where E_i is the individual cell energy, E_{tot} is the total energy in all cells, and $\mathcal{C}$ is a constant. In this way, an effective cutoff is introduced on individual hits, and only cells which contain a high percentage of the event energy contribute to the reconstruction.

The polar resolution, σ_θ, and the polar bias, $\Delta\theta$, are, respectively, the root-mean-square and the most probable value of the distribution of the difference between the reconstructed and the generated polar angles. The existence of $\Delta\theta$ is due to the non-linear transformation between the global coordinate system of the detector, and the coordinate system of LumiCal (aligned with the outgoing beam), in which the shower position is reconstructed. There is an optimal value for $\mathcal{C}$, for which σ_θ is minimal. This is shown in Fig. 6a using 1.5 TeV electron showers. The corresponding values of $\Delta\theta$ are presented in Fig. 6b. Accordingly, the polar resolution and bias of LumiCal are

$$\sigma_\theta = (2.5 \pm 0.01) \cdot 10^{-5} \text{ rad}, \quad \Delta\theta = (2.4 \pm 0.1) \cdot 10^{-5} \text{ rad}, \tag{9}$$

respectively.

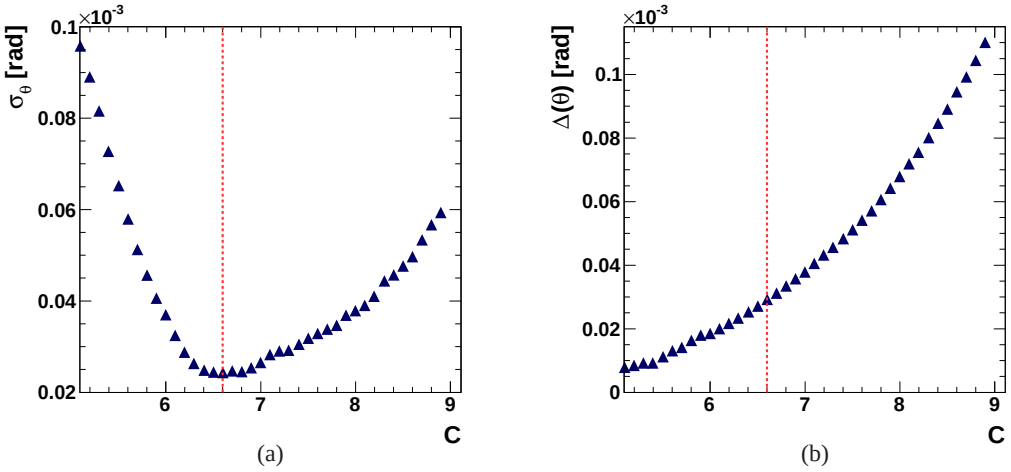

Figure 6: The polar resolution, σ_θ, (a) and the polar bias, $\Delta\theta$, (b) as a function of the logarithmic weighing constant, $\mathcal{C}$, using 1.5 TeV electron showers. The dashed lines mark the optimal value of $\mathcal{C}$.

2.5 Uncertainty in the Luminosity Measurement

The luminosity is measured with a *statistical uncertainty* in the counting of N_B, the number of Bhabha scattering events. The relative uncertainty may be expressed as

$$\left(\frac{\Delta\mathcal{L}}{\mathcal{L}}\right)_{stat} = \frac{\Delta N_B}{N_B} = \frac{\sqrt{N_B}}{N_B} = \frac{1}{\sqrt{N_B}}\,. \tag{10}$$

It will be shown (Fig. 13 below) that for the current design of LumiCal, $(\Delta\mathcal{L}/\mathcal{L})_{stat}$ is below the required bound on the uncertainty for the luminosity measurement.

In addition to the statistical uncertainty, there is also uncertainty in the luminosity measurement due to the relative *reconstruction bias*,

$$\left(\frac{\Delta\mathcal{L}}{\mathcal{L}}\right)_{rec} \approx 2\frac{\Delta\theta}{\theta^f_{min}}\,, \tag{11}$$

which is a consequence of the polar bias [7].

The analytic approximation of Eq. (11) has been shown to hold well [21]. Its implication is that $\Delta\theta$ and θ^f_{min} are the two most important parameters that affect the precision of the luminosity measurement. The steep fall of the Bhabha cross-section with the polar angle translates into significant differences in the counting rates of Bhabha events, for small changes in the angular acceptance range.

In practice it is possible to control the uncertainty of the polar reconstruction by measuring the polar bias in a test-beam. If this is done, $\Delta\theta$ in Eq. (11) becomes the uncertainty of this measurement and reduces significantly compared to the intrinsic polar bias (Eq. (9)). In the following we shall ignore this possibility and treat $(\Delta\mathcal{L}/\mathcal{L})_{rec}$ as if a measurement of $\Delta\theta$ were not possible. It will be shown (Fig. 8 below) that even in this worst-case scenario, the uncertainty in the luminosity measurement is smaller than the design goal.

3 Design Parameters of LumiCal

3.1 Layer Segmentation Scheme

In order to determine the optimal set of geometrical parameters for LumiCal, one has to balance between the need to achieve the design goal for the luminosity measurement along with several constraining factors. In the following the reasons for choosing the current detector design are presented. It will be shown that the parameter which influences the luminosity measurement the most, is the number of radial divisions, which determines the angular resolution of LumiCal.

The Number of Radial Divisions

For different radial cell sizes one needs to re-optimize the logarithmic weighing constant, $\mathcal{C}$, of Eq. (8), as the distribution of deposited energy in a single cell changes for each case. The polar resolution and bias are plotted in Fig. 7 as a function of the angular cell size, ℓ_θ. In each case the appropriate optimal value of $\mathcal{C}$ was used. The errors shown in the figure for σ_θ and for $\Delta\theta$ are derived from the errors on the fit parameters of, respectively, the root-mean-square and the most probable value of the distribution of the difference between the reconstructed and the generated polar angles. The relative bias in the luminosity measurement, $(\Delta\mathcal{L}/\mathcal{L})_{rec}$, for the respective values of the polar bias are shown in Fig. 8. The relative bias is smaller than the design goal of 1 % for the entire range of ℓ_θ which is shown, and in particular for the baseline cell size, $\ell_\theta = 2$ mrad.

Both σ_θ and $\Delta\theta$ become smaller as the angular cell size decreases. The relative bias in luminosity follows the same trend. This is due to the fact that the bounds on the fiducial volume do not strongly depend on the number of radial divisions. Consequently the same value for the minimal polar angle, $\theta^f_{min} = 50$ mrad, was used for all of the points in Fig. 8.

When the number of channels increases, problems such as cross-talk between channels, power consumption issues and the need for cooling, arise. It is therefore advisable to keep the number

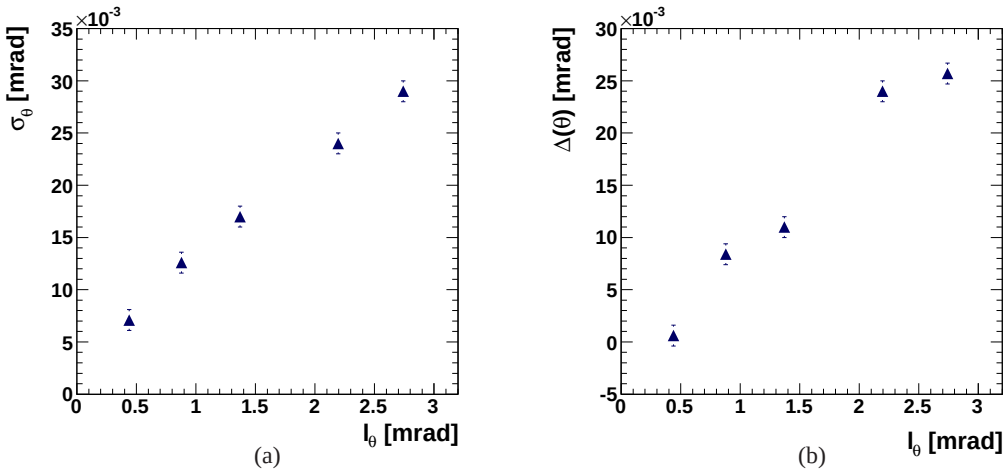

Figure 7: The polar resolution, σ_θ, (a) and the polar bias, $\Delta\theta$, (b) for the appropriate optimal logarithmic weighing constants, as a function of the angular cell size, ℓ_θ. Electron showers of 1.5 TeV were used.

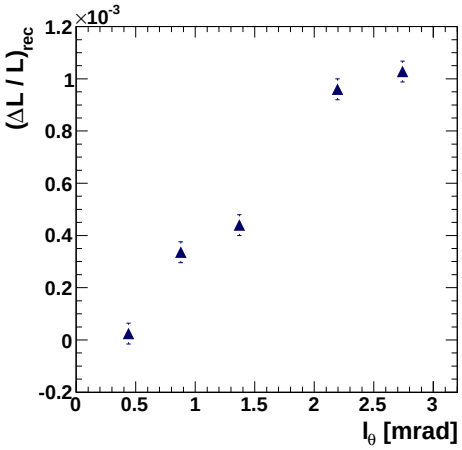

Figure 8: Relative reconstruction bias in the luminosity measurement, $(\Delta\mathcal{L}/\mathcal{L})_{rec}$, as a function of the angular cell size, ℓ_θ, for the values of the polar bias presented in Fig. 7b.

of cells as low as possible. The chosen baseline number of 50 radial divisions is, therefore, a compromise between minimizing the relative luminosity uncertainty, and limiting the number of channels.

The Number of Azimuthal Divisions

The number of azimuthal divisions does not affect the reconstruction of the polar angle. The energy resolution does not depend on the number of channels either, since energy contributions are integrated over all of the cells. In addition, rounding errors, due to digitization of the signal, are small for the range of cell sizes which is being considered (see [22]).

The importance of constraining the azimuthal cell size is in improving the resolving power of LumiCal for distinguishing between multiple simultaneous showers. Strictly speaking, Born-level elastic Bhabha scattering never occurs. In practice, the process is always accompanied by the emission of electromagnetic radiation, $e^+e^- \to e^+e^-\gamma$. The ability to distinguish between a radiative photon and its accompanying lepton is determined by the resolving capabilities of the detector, and is a function of the angular separation between the two particles. When the two can be separated, then the experimental measurement of the number of radiative photons can be compared with the theoretical prediction, and thus the theory can be partly tested.

A clustering algorithm has been developed in order to facilitate this goal [23, 7]. The conclusion was that there is a bound on the minimal azimuthal cell-length. For the present distance of 2.27 m, 48 azimuthal divisions constitute the lower bound.

3.2 Readout Scheme

For a given granularity of LumiCal, it is necessary to define the dynamic range of the electronics required to process the signal from the detector.

The output of MOKKA is given in terms of energy lost in the active material, silicon in the case of LumiCal. In order to translate the energy signal into units of charge, the following formula is used:

$$\mathcal{S}_Q[\mathrm{fC}] = \frac{1.6\cdot 10^{-4}}{3.67}\,\mathcal{S}_\mathcal{E}[\mathrm{eV}], \tag{12}$$

where $\mathcal{S}_\mathcal{E}$ denotes the signal in units of eV, and $\mathcal{S}_Q$ the signal in units of fC. The value 3.67 eV is the energy to create an electron-hole pair in silicon. The number $1.6\cdot 10^{-4}$ fC is the charge of an electron.

In order to determine the lower bound on the signal in LumiCal, the passage of muons through the detector was simulated. Muons do not shower, and are, therefore, minimum ionizing particles (MIPs). Muons may be used to inter-calibrate the cells of the detector, and may also be used to check *in-situ* the alignment of the detector. The distribution of the energy deposited in a detector cell by 250 GeV muons is presented in Fig. 9. Accordingly, the most probable value (MPV) of induced charge for a muon traversing 300 μm of silicon is 89 keV, which is equivalent to 3.9 fC.

The signature of a Bhabha event is an e^+e^- pair, where the leptons are back to back and carry almost all of the initial energy. Subsequently, for $\sqrt{s} = 500$ GeV (3 TeV) the maximal energy

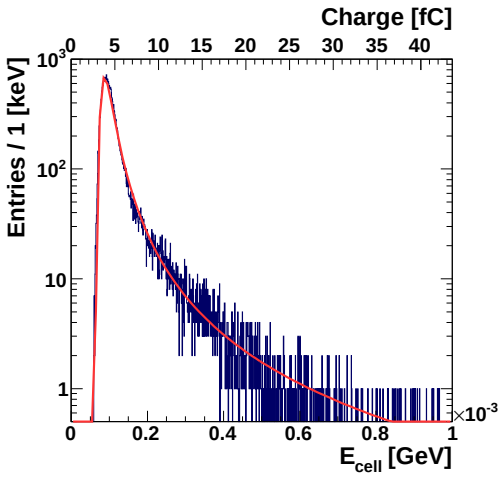

Figure 9: Distribution of the energy deposited in a detector cell, E_{cell}, by 250 GeV muons. A corresponding scale in units of charge is also shown.

to be absorbed in LumiCal is 250 GeV (1.5 TeV), and therefore electron showers of 250 GeV (1.5 TeV) may be used in order to determine the upper bound on the signal. The amount of energy which is deposited in a single detector cell also depends on the size of the cell, as can be observed in Fig. 10. The figure presents the distribution of collected charge per cell for 250 GeV and for 1.5 TeV electron showers for a LumiCal with 100 or 50 radial divisions, which correspond to angular cell sizes of 0.9 and 2 mrad, respectively. The number of azimuthal cells was set at the baseline number, 48. The distribution of the maximal charge collected in a single cell per shower for the different setups is also shown.

One can observe that the dependence of the distributions on the energy of the shower is linear, as expected from Fig. 5. For the baseline case of 50 radial divisions and $\sqrt{s} = 3$ TeV, the charge distribution in a single cell extends up to 50 pC. The dynamic range of the signal for $\sqrt{s} = 3$ TeV is therefore $3.9 < C_{cell} < 50 \cdot 10^3$ fC. In practice it may be possible to set the low bound at values higher than 1 MIP, if the measurement of single MIPs is not required[1)]. The maximal value of the low bound should be such that the energy resolution of LumiCal is not degraded. Further study of this issue in the future is warranted. It is also possible to divide the dynamic range into low- and high-gain regions, and to have separate digitization in each region. A study of this nature is presented in [22].

3.3 The Number of Layers

A distribution of the energy deposited in a layer, E_ℓ, by electron-showers of different energies, E_{sh}, are presented in Fig. 11a. The dependence of the energy resolution of 1.5 TeV electron

[1] This, however, would exclude the possibility of calibrating the detector with muons.

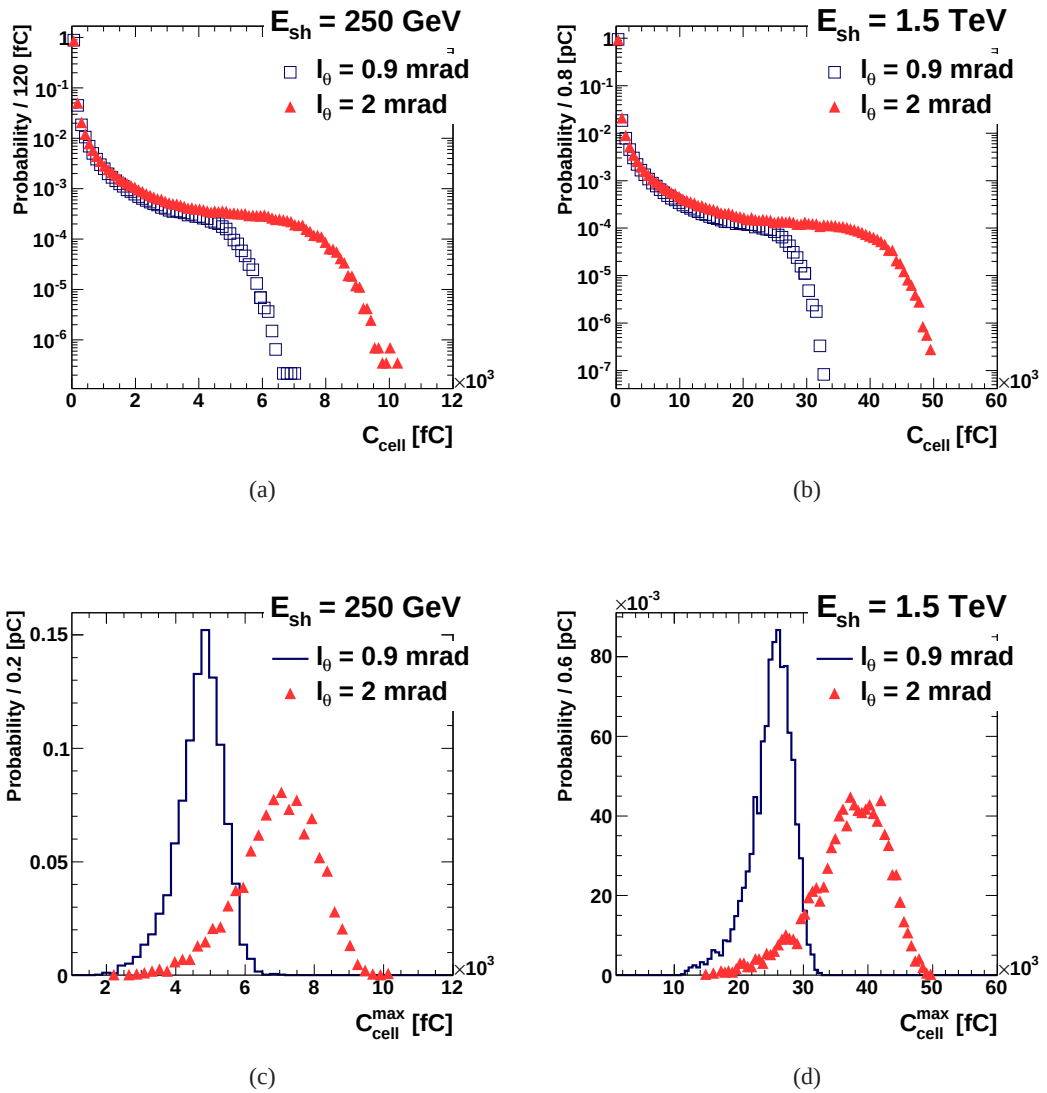

Figure 10: (a) and (b): Normalized distributions of the charge deposited in a detector cell, C_{cell}, by 250 GeV and by 1.5 TeV electron showers for a LumiCal with two alternative angular cell sizes, $\ell_\theta = 0.9$ or 2 mrad, as denoted in the figures. (c) and (d): Normalized distributions of the maximal charge collected in a single cell per shower, C_{cell}^{max}, corresponding to the distributions shown in (a) and (b), respectively.

showers on the number of layers, N_ℓ, is shown in Fig. 11b, where the errors were computed as for Fig. 3. It is apparent from the two figures that the amount of energy which leaks through the back layer of LumiCal is insignificant for $N_\ell \geq 40$. It was, therefore, decided that 40 layers (40 X_0) are sufficient for the containment of showers with $E_{sh} \leq 1.5$ TeV.

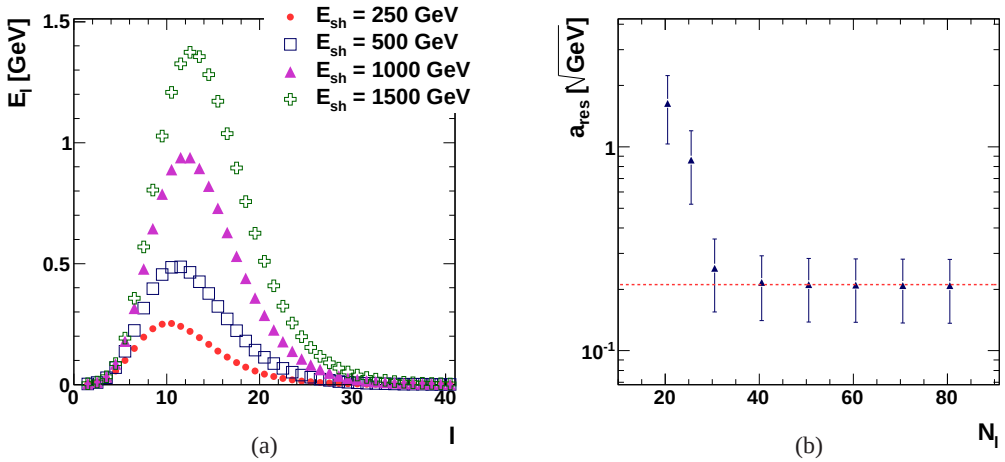

(a) (b)

Figure 11: (a) Distributions of the energy deposited in LumiCal, E_ℓ, as a function of the layer number, ℓ, for various shower energies, E_{sh}, as indicated in the figure. (b) Dependence of the energy resolution, a_{res}, on the number of layers in LumiCal, N_ℓ, using 1.5 TeV electron showers. The dashed line marks the nominal value of the energy resolution, $a_{res}(N_\ell = 40) = 0.21\ \sqrt{\text{GeV}}$.

3.4 The Inner Radius

In order to determine the optimal values for the inner radius of LumiCal, R_{min}, several facts need to be considered.

- The cross-section of Bhabha scattering drops rapidly with the polar angle, and therefore R_{min} should be made as low as possible.
- The spectrum of incoherent pairs, which carries high radiation doses that can harm the sensors of LumiCal, peaks at low angles. Therefore R_{min} should be made large enough to avoid the pair radiation.
- As the number of incoherent pairs which hit LumiCal increases, so does the amount of backscattering from LumiCal into the inner region of the detector. This backscattering is harmful and should be minimized.

In the following we address these issues.

3.4.1 Statistical Uncertainty in Counting the Number of Bhabha Events

For small angles ($\leq 10^\circ$), Bhabha scattering is dominated by the t-channel exchange of a photon [24]. One can write the differential cross-section as

$$\frac{d\sigma_{\rm B}}{d\theta} = \frac{2\pi\alpha_{em}^2}{s}\frac{\sin\theta}{\sin^4(\theta/2)} \approx \frac{32\pi\alpha_{em}^2}{s}\frac{1}{\theta^3}\,, \tag{13}$$

where the scattering angle, θ, is the angle of the scattered lepton with respect to the beam, α_{em} is the fine structure constant, and s is the center-of-mass energy squared.

The dependence of the Bhabha cross-section on the polar angle is shown in Fig. 12 for $\sqrt{s} = 500$ GeV and 3 TeV. The dashed lines mark the fiducial volume of LumiCal, $50 < \theta^f < 130$ mrad. The integrated cross-section within the fiducial volume is $\sigma_{\rm B} = 1457$ and 42 pb for $\sqrt{s} = 500$ GeV and 3 TeV respectively. Both distributions have the same polar dependence and scale with s, in accordance with Eq. (13). The values of $\sigma_{\rm B}$ presented here were computed for Bhabha events which complied with the condition that, for a given scattering event, both the polar angle of the electron and that of the positron must lie within the fiducial volume. This is due to the fact that the luminosity is measured using selection cuts (see Sect. 4), which include this constraint.

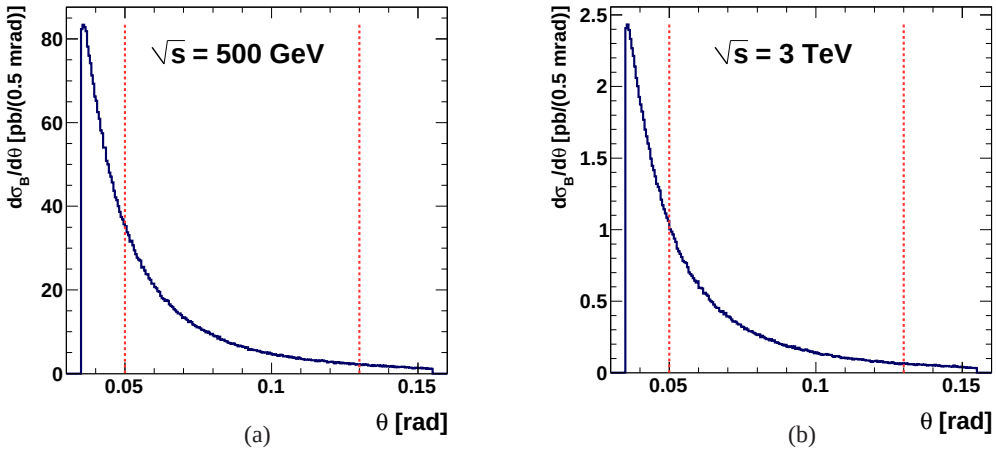

(a) (b)

Figure 12: Dependence of $\sigma_{\rm B}$, the Bhabha cross-section, on the polar angle, θ, for two center-of-mass energies, $\sqrt{s} = 500$ GeV and 3 TeV, as indicated in the figures. The dashed lines mark the fiducial volume of LumiCal, $50 < \theta^f < 130$ mrad.

The statistical uncertainty in counting the number of Bhabha events, $(\Delta\mathcal{L}/\mathcal{L})_{stat}$, depends on N_B, the number of events which are counted (Eq. (10)). As the inner radius of LumiCal is made larger, the fiducial volume becomes smaller, and so N_B becomes smaller. Figure 13 shows

the dependence of $(\Delta\mathcal{L}/\mathcal{L})_{stat}$ on the minimal polar angle, which defines the low edge of the fiducial volume, for $\sqrt{s} = 500$ GeV and 3 TeV. The maximal polar angle was kept constant at 130 mrad for all cases. An integrated luminosity of 100 fb^{-1} was assumed, along with a pessimistic Bhabha selection efficiency of 50 % (see Sect. 4). The uncertainty is smaller than 0.03 % (0.2 %) for $\sqrt{s} = 500$ GeV (3 TeV) for all choices of θ_{min} presented here. In particular for $\theta_{min} = \theta^{f}_{min} = 50$ mrad the uncertainty is lower than required by the design goal.

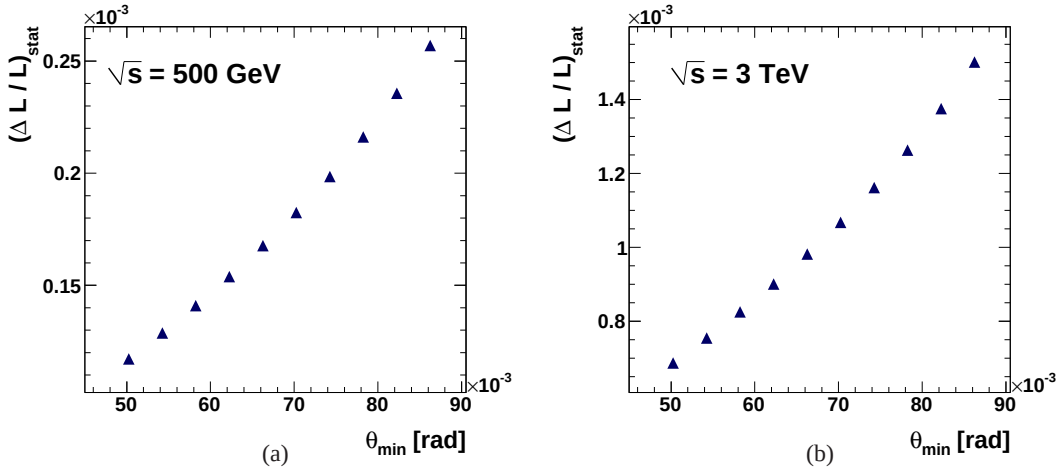

Figure 13: Dependence of the statistical uncertainty in counting the number of Bhabha events, $(\Delta\mathcal{L}/\mathcal{L})_{stat}$, on the minimal polar angle, θ_{min}, which defines the low edge of the fiducial volume in each case. The relation is shown for two center-of-mass energies, $\sqrt{s} = 500$ GeV and 3 TeV, as indicated in the figures. An integrated luminosity of 100 fb^{-1} and a Bhabha selection efficiency of 50 % were assumed.

3.4.2 Beam Background

At CLIC, the beam-beam effect between the colliding electron and positron bunches is much stronger than at the ILC [25]. On average, more than two photons per electron/positron are produced [8]. Some of these photons are converted into high energy coherent pairs (which will mostly exit into the post-collision line), others into lower energy incoherent pairs (some of which will end up in LumiCal). Therefore, prior to the Bhabha scattering, the interacting particles are likely to have been deflected, and their energy to have been reduced.

In the current accelerator design a crossing angle of 20 mrad is foreseen between the incoming and outgoing beam lines [8]. In the *anti-detector integrated dipole* (anti-DID) field configuration, the magnetic field is directed along the outgoing beam lines with a kink at the transverse plane containing the IP. This setup should be distinguished from the alternative *solenoid* field configuration, where the magnetic lines are directed along the symmetry axis of the detector. A

schematic representation of the two field configurations, taken from [26], is shown in Fig. 14.

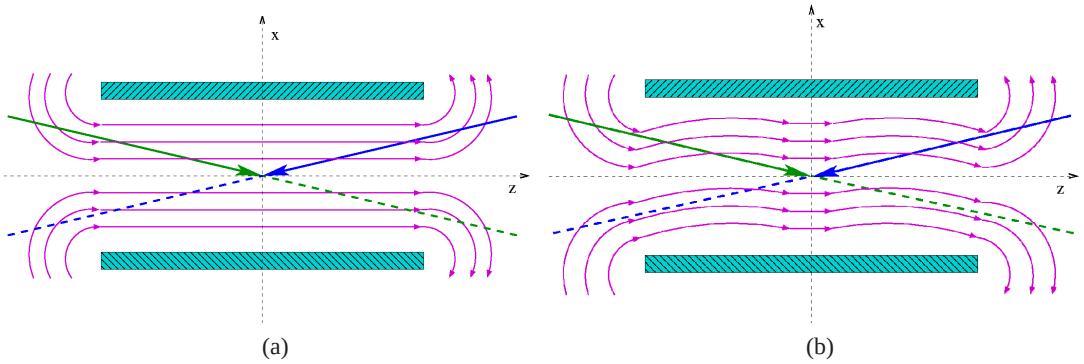

Figure 14: Schematic representation of the solenoid (a) and anti-DID (b) magnetic field configurations. The solid curves represent the magnetic field lines, the solid arrows represent the incoming beams and the dashed arrows represent the outgoing beams.

Energy Deposits in LumiCal

Figures 15a and 15b show scatter plots in the xy-plane of the energy of incoherent pairs which traverse the first layer of LumiCal. The energy spectrum is shown for the solenoid and for the anti-DID magnetic field configurations. The distribution of pairs corresponds to that which will be created in 10 bunch-crossings (BX) at nominal beam conditions, which include a magnetic field of 4 T and a crossing-angle of 20 mrad. The nominal center-of-mass energy is $\sqrt{s} = 3$ TeV [8]. The distribution of the incoherent pairs in the solenoid configuration is more widespread compared to the anti-DID case. Figure 15c shows the dependence of the energy of the pairs distribution on the distance from the center of LumiCal. The position of the center is $\{x_0, y_0\} = \{2.27, 0\}$ cm, where the x-coordinate is shifted due to the crossing angle. While the symmetric energy distribution for the anti-DID case falls off at slightly lower radii compared to the solenoid case, both distributions peak away from the inner radius of LumiCal. The amount of energy in both setups decreases as the distance from the center grows. The inner radius of LumiCal was set to 10 cm in order to keep a small safety margin from the region where the energy deposition by the pairs is large in either case.

Figures 16a and 16b present a scatter plot of the deposited energy in LumiCal due to incoherent pairs from 10 BX. The energy is integrated over all layers of LumiCal. The energy distributions are shown for two magnetic field configurations, solenoid and anti-DID. In Fig. 16c the deposited energy due to incoherent pairs from 10 BX as a function of the polar angle and of the layer number is shown. The inner radius of LumiCal was set to the baseline value of 10 cm, and the magnetic field is in the anti-DID configuration. The equivalent distribution for the solenoid field (not shown) is not significantly different. Most of the energy is deposited in the front layers

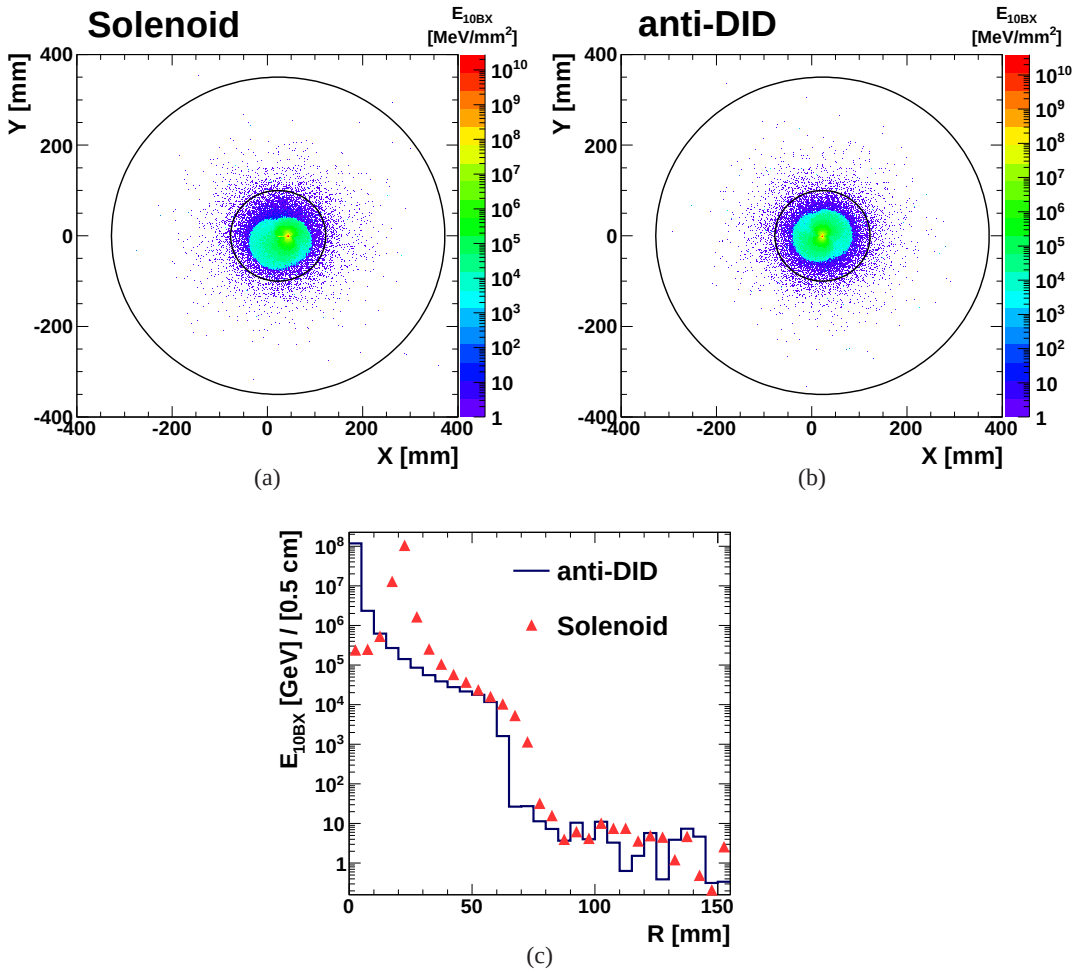

Figure 15: (a) and (b): Scatter plot in the xy-plane of the energy of incoherent pairs from 10 BX, which cross the first layer of LumiCal, $E_{10\mathrm{BX}}$. The black circles represent the inner and outer radii of LumiCal, 10 and 35 cm respectively. (c): Dependence of the energy of the pairs distribution, which is shown in the top figures, on the distance from the center of LumiCal. A magnetic field of 4 T and a crossing-angle of 20 mrad were simulated at $\sqrt{s} = 3$ TeV. The energy distributions are shown for two magnetic field configurations, solenoid and anti-DID, as indicated in the figures.

of LumiCal at low angles. From this it is evident that both the number of particles and the energy of individual particles is reduced with increasing polar angle.

Figure 17 shows the deposited energy in LumiCal due to incoherent pairs from 10 BX as a function of the layer number for the two field configurations. The energy distributions are shown for four different inner radii of LumiCal, $R_{min} = 4,\ 6,\ 8$ and 10 cm. For the solenoid

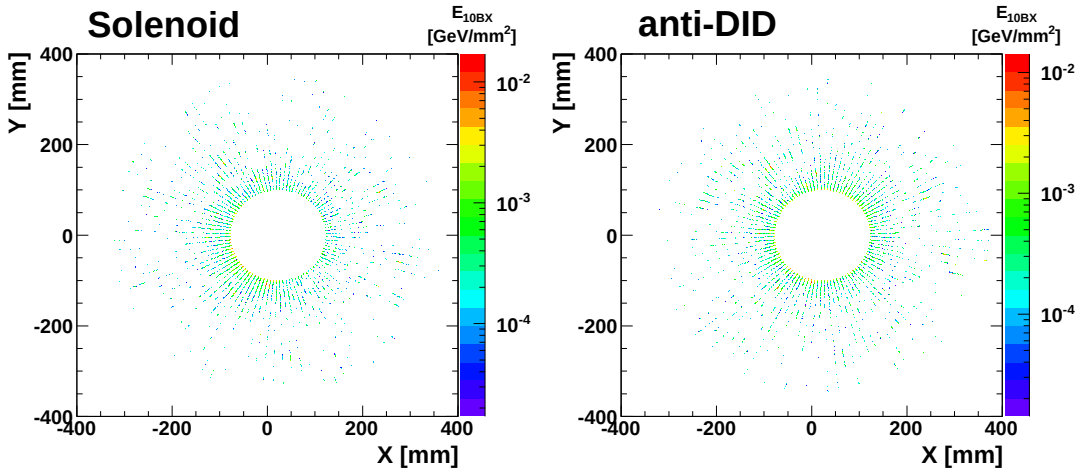

(a) (b)

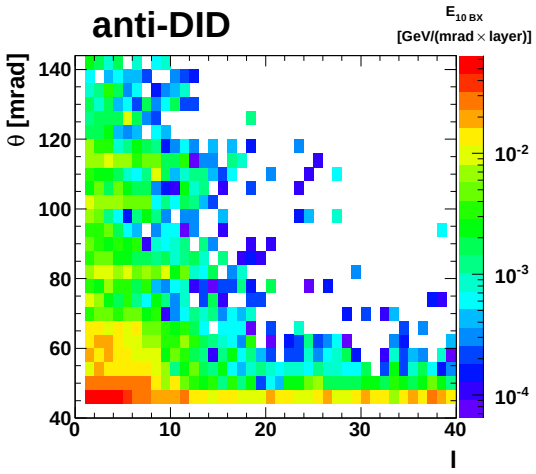

(c)

Figure 16: (a) and (b): Energy spectrum of the deposited energy in LumiCal due to incoherent pairs from 10 BX. The energy is integrated over all layers of LumiCal and shown in the xy-plane. A magnetic field of 4 T and a crossing-angle of 20 mrad were simulated at $\sqrt{s} = 3$ TeV. The energy distributions are shown for two magnetic field configurations, solenoid and anti-DID, as indicated in the figures. (c): Dependence of the deposited energy in LumiCal, using the anti-DID field configuration, as a function of the polar angle, θ, and of the layer number, ℓ.

field the smallest value of R_{min} which can be allowed is 10 cm. For the anti-DID case both $R_{min} = 8$ and 10 cm are acceptable. This is evident by the fact that for the higher values of R_{min} the amount of energy which is deposited in LumiCal by the pairs is comparable or much larger than the energy signature of Bhabha events (see Fig. 18 below).

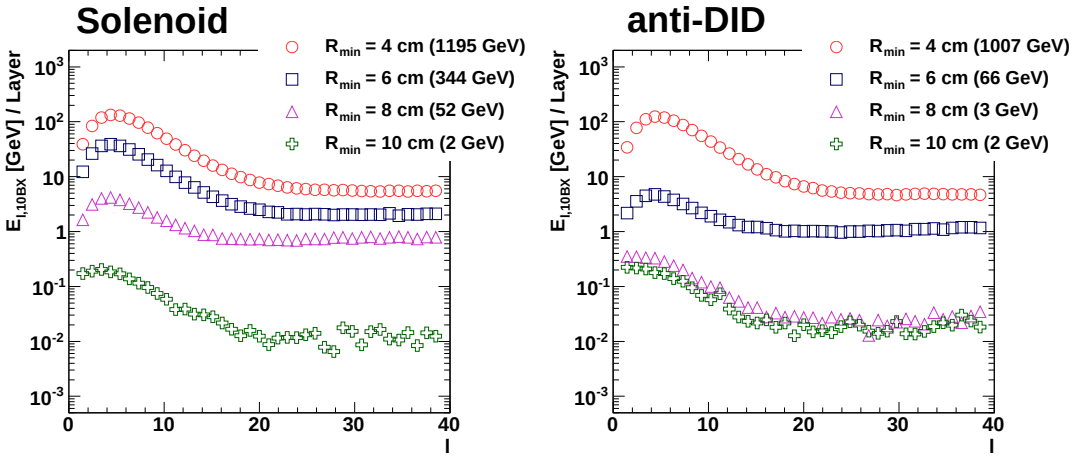

(a) (b)

Figure 17: Deposited energy in LumiCal due to incoherent pairs from 10 BX, $E_{\ell,10BX}$, as a function of the layer number, ℓ. A magnetic field of 4 T and a crossing-angle of 20 mrad were simulated at $\sqrt{s} = 3$ TeV. As indicated in the figures, two magnetic field configurations, solenoid and anti-DID, and four different inner radii of LumiCal, $R_{min} =$ 4, 6, 8 and 10 cm, were used. The numbers in the brackets represent the total amount of energy which was deposited in LumiCal in each case.

The *background-to-signal* ratio is defined as

$$B/S \equiv \frac{E_b}{E_s} \tag{14}$$

where E_b (E_s) represents the energy deposits by the background (signal) process in a given configuration. One may also define the background-to-signal ratio for a layer ℓ in LumiCal, $(B/S)_\ell$, by considering the energy deposits by the background and signal processes in a given layer.

The deposited energy as a function of the layer number for $R_{min} = 10$ cm is presented in Fig. 18a. Shown there are the energy distributions for incoherent pairs in the two field setups along with the corresponding distribution of a 1.5 TeV electron shower, which compares with the signature of a Bhabha event. Figures 18b shows the dependence of $(B/S)_\ell$ on the layer number, where the signal in this case is represented by the 1.5 TeV electron shower. The distributions of the incoherent pairs is shown for the two magnetic field configurations and for 10 and 312 bunch crossings.

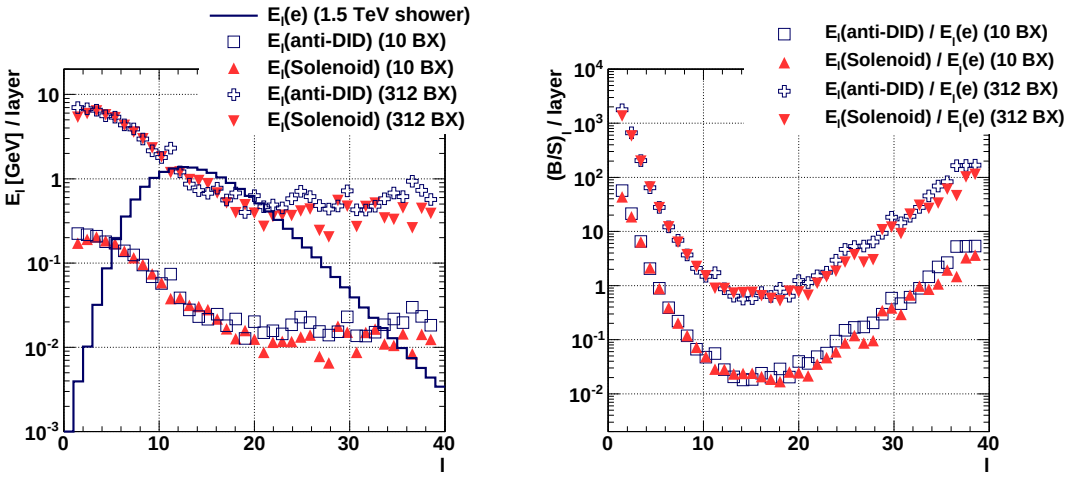

Figure 18: Deposited energy, E_ℓ, (a) and background-to-signal ratio, $(B/S)_\ell$, (b) as a function of the layer number, ℓ. As indicated in the figures, the following distributions are used: the depositions of incoherent pairs in a solenoid magnetic field configuration, $E_\ell(\text{Solenoid})$, from 10 and from 312 BX, the depositions of incoherent pairs in an anti-DID field configuration, $E_\ell(\text{anti}-\text{DID})$, from 10 and from 312 BX and the depositions by a 1.5 TeV electron shower, $E_\ell(\text{e})$.

The amount of background energy which is deposited in LumiCal depends on the number of bunch-crossings which are read out simultaneously. Currently, the time-stamping resolution for CLIC is unknown. Figure 18 therefore presents both the distributions of deposited pair energy for 10 BX and for a full bunch-train of 312 BX. We consider first the possibility that the signal is integrated over 10 BX. In this case, at $8 < \ell < 28$, where the electron shower peaks, the amount of energy deposited by the pairs compared to the electron shower is small, with $B/S = \mathcal{O}(10^{-1})$ per layer. If, however, an entire bunch-train (312 BX) is read out at once, then $B/S = \mathcal{O}(1)$ in the region where the electron shower peaks. In the latter case it may, therefore, be difficult to distinguish between the signal of Bhabha events and the energy deposits of the incoherent pairs.

According to Fig. 16c, most of the energy is deposited either at very low angles in all layers, or at high angles in the first few layers. In addition, it should be noted that on the one hand, the fiducial volume cut eliminates showers which develop at very small angles, while on the other hand, since high energy electron showers peak at the inner layers of LumiCal, the information from the first layers is less important. It is, therefore, possible to perform a cut on a significant amount of the energy deposited by the incoherent pairs, and thus reduce the respective values of B/S further. Additional study of this issue is warranted.

Backscattering from the Front Layer of LumiCal

Figure 19 presents the energy spectrum of backscattered particles from the front face of LumiCal for 10 BX at $\sqrt{s} = 3$ TeV. A magnetic field of 4 T in a solenoid configuration and a crossing-angle of 20 mrad were used. Several inner radii of LumiCal, $R_{min} = 4,\ 7$ and 10 cm, were simulated.

It is apparent that the amount of backscattering for low radii is significantly larger compared to $R_{min} = 10$ cm. One should keep in mind, though, that these results do not show which sub-detector is hit by the backscattered particles. In order to determine the number of hits and the deposited energy in the vertex and tracking detectors by backscattered particles, a full simulation of the detector is needed.

3.4.3 Discussion of the Results

Two conflicting trends need to be considered in order to determine the optimal value of the inner radius of LumiCal. On the one hand one would like to set R_{min} as low as possible in order to increase the percentage of the Bhabha cross-section inside the fiducial volume of LumiCal. On the other hand, for low values of R_{min} both the beam background and the backscattering from LumiCal increase.

The amount of beam background in LumiCal depends on the configuration of the magnetic field. For the solenoid setup the amount of incoherent pairs deposited at low radii in LumiCal is large compared to the anti-DID configuration. For $R_{min} = 10$ cm the differences when comparing the two field types are minimal. The anti-DID field configuration is preferable to the solenoid setup, since it allows for more leeway in calibration of the magnetic field; it gives a safety margin between the distribution of pairs and LumiCal. This can be deduced from the fact that the amount of pair energy at $R = 8$ cm in the anti-DID configuration is significantly smaller than the comparable distribution for the solenoid case.

The amount of backscattering also drops significantly for $R_{min} = 10$ cm compared to lower values. Since the statistical uncertainty on the luminosity measurement for $R_{min} = 10$ cm is smaller than the design goal, we conclude that this is an acceptable value. It should be emphasized that a full simulation of the entire detector is needed in order to determine that the residual backscattering for $R_{min} = 10$ cm is indeed acceptable, and that the performance of the vertex and tracking detectors correspond to the physics requirements.

3.5 The Outer Radius

The outer radius of LumiCal, R_{max}, is less constrained than the inner radius. The two major concerns are the total radial size of LumiCal, and the size of the integrated Bhabha cross-section in the fiducial volume.

As discussed in Sect. 3.1, in order to perform clustering in LumiCal, it is necessary to be able to distinguish between EM showers initiated by different particles. The study described in [23,7]

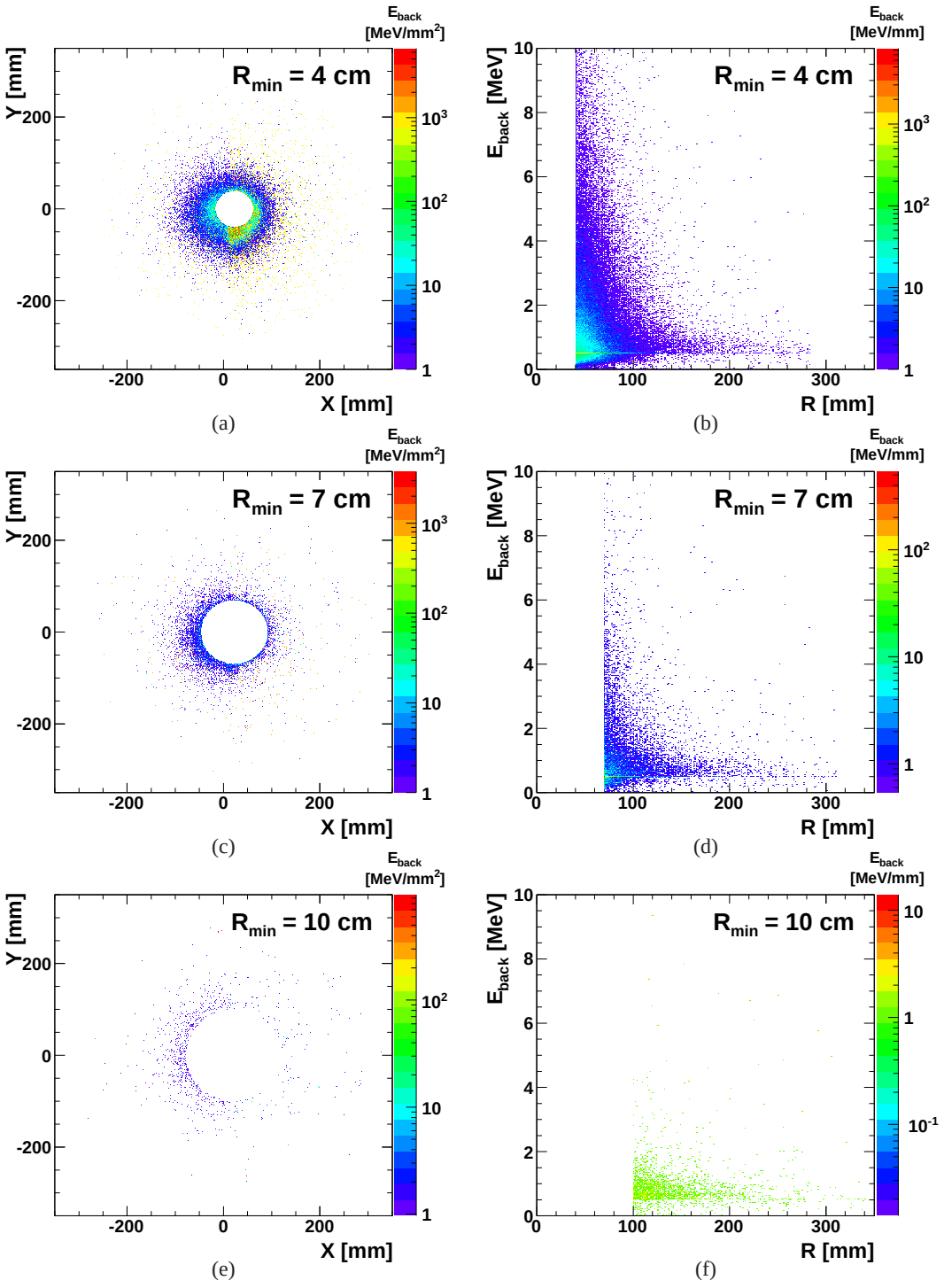

Figure 19: Energy spectrum of backscattered particles from the front face of LumiCal for 10 BX at $\sqrt{s} = 3$ TeV in a 4 T solenoid magnetic field. Several values of the inner radius of LumiCal, R_{min}, were selected, as indicated in the figures. (a), (c) and (e): Scatter plots of the energy of backscattered particles, E_{back}, in the xy-plane. (b), (d) and (f): Scatter plots of E_{back} as a function of the distance from the center of LumiCal, R.

showed that in most cases a separation of at least one Molière radius between a pair of showers is needed in order to resolve each shower, where $R_{\mathcal{M}} \approx 1.5$ cm. It was subsequently concluded in the study that the total radial size of LumiCal should not be smaller than several Molière radii.

In this context we consider the integrated Bhabha cross-section within the fiducial volume of LumiCal, σ_{B}. As can be deduced from Fig. 12, σ_{B} becomes small at large angles. It may, therefore, be inferred that taking into account events within this angular region does not reduce the statistical uncertainty significantly. For instance, we may consider a geometry where $R_{max} =$ 25 cm, for which the total radial size of LumiCal is 10 $R_{\mathcal{M}}$. In this case the physical polar size of LumiCal is 44 to 110 mrad and the *reduced fiducial volume* is roughly $50 < \theta^{f}_{red} <$ 90 mrad. The statistical uncertainty in counting the number of Bhabha events may now be computed for the reduced fiducial volume. Assuming an integrated luminosity of 100 fb^{-1} and a Bhabha selection efficiency of 50 % (as for Fig. 13), the subsequent statistical uncertainty in the luminosity measurement is 0.08 % at $\sqrt{s} = 3$ TeV. We therefore find that even for the reduced fiducial volume, the uncertainty is an order of magnitude lower than required.

In conclusion, the nominal value of the outer radius ($R_{max} = 35$ cm) may be reduced, if it becomes necessary due to external constraints, such as the Forward Tracking. Care would have to be taken in order to verify that the total radial size of LumiCal always remains larger than a few Molière radii. In addition, the integrated Bhabha cross-section within the reduced fiducial volume should not decrease too much, so that the subsequent statistical uncertainty in the luminosity measurement remains small. It should also be noted that if the size of R_{max} is changed, the number of radial divisions will have to be modified as well, so that the radial size of cells does not exceed 2 mrad, as discussed in Sect. 3.1.

4 Physics Background and Selection Cuts

4.1 Methodology

Four-fermion neutral current processes $e^-e^+ \to l^-l^+$ ($l = e, \mu$) and $e^-e^+ \to q^-q^+$ ($q = u, d, c, s, b$) are considered to be the main source of physics background for the luminosity measurement. They are dominated by the multiperipheral processes (2-photon exchange). The contributing four-fermion Feynman diagrams are given in Fig. 20.

A set of topological cuts is applied in order to distinguish Bhabha scattering from the background processes. This is done by comparing the position and the energy of EM showers, which are initiated in the two arms of LumiCal by the scattered particles [27, 21].

In a typical Bhabha scattering event multiple showers develop in each arm of LumiCal, due to the emission of final-state radiation. In the current detector configuration there is no way to distinguish between showers which are initiated by leptons and those which are attributed to photons. Therefore, in order to retain a consistent picture, the showers of all of the particles which are within the fiducial volume of LumiCal are clustered together. The selection cuts then compare between the properties of the clustered showers in the two arms of the detector.

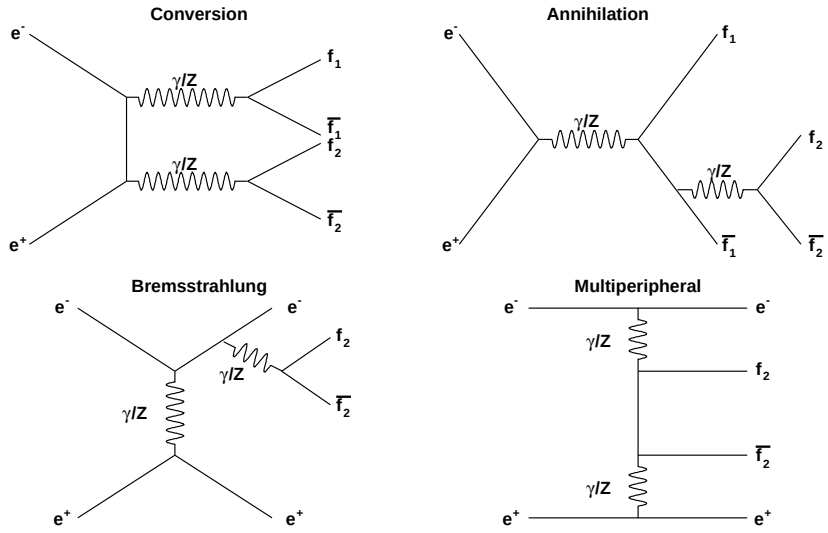

Figure 20: Feynman diagrams contributing to neutral current four-lepton production. The dominant fraction is described by the multi-peripheral diagram (bottom right).

We define the *relative energy cut*,

$$\frac{\Delta E_{r,l}}{E_{r,l}} \equiv \frac{|E_r - E_l|}{\min\{E_r, E_l\}}, \tag{15}$$

and the *polar angle cut*,

$$\Delta\theta_{r,l} \equiv |\theta_r - \theta_l|, \tag{16}$$

where E_r and E_l (θ_r and θ_l) are, respectively, the energy (polar angle) of the clustered shower in the right and left arms of LumiCal. We then demand that the values of the two cuts be larger than some given constants, $\mathcal{C}_E$ and $\mathcal{C}_\theta$, for each event considered. In addition to the topological cuts, the polar angle in either arm must lie within the fiducial volume. The three restrictions can be summarized as

$$\frac{\Delta E_{r,l}}{E_{r,l}} \leq \mathcal{C}_E \qquad |\theta_r - \theta_l| \leq \mathcal{C}_\theta \qquad \theta^f_{min} \leq \theta_r, \theta_l \leq \theta^f_{max}. \tag{17}$$

Only events that pass the cuts are counted as Bhabha scattering events.

One may define the *selection efficiency* and the *background-to-signal ratio of selection* of Bhabha events as

$$\mathcal{E}_{cut} \equiv \frac{N_{Bh}(\text{cut})}{N_{Bh}(\text{all})} \qquad (B/S)_{cut} \equiv \frac{N_{bkg}(\text{cut})}{N_{Bh}(\text{cut})}, \tag{18}$$

respectively. The symbol $N_{Bh}(\text{all})$ represents the number of Bhabha events which were simulated, while $N_{Bh}(\text{cut})$ and $N_{bkg}(\text{cut})$ are, respectively, the number of Bhabha and the number of background events which passed the selection cuts.

As the selection cuts become more loose, both $\mathcal{E}_{cut}$ and $(B/S)_{cut}$ grow, since more events from both Bhabha scattering and background sources pass the cuts. As $\mathcal{E}_{cut}$ becomes smaller, the statistical uncertainty of counting the number of Bhabha scatterings grows (see Eq. (10)). One the other hand, as $(B/S)_{cut}$ grows, the relative bias in counting grows (see Eq. (2)). For the optimal set of cuts, the value of $\mathcal{E}_{cut}$ will be as large as possible and the value of $(B/S)_{cut}$ will be as small as possible. One therefore has to find the middle ground between the two conflicting trends.

As discussed in Sect. 3.4.2, prior to the Bhabha scattering, the interacting particles in each bunch are likely to have been deflected due to interaction with the opposite bunch [25]. In order to account for this, the polar angle cut shall be adapted. A possible method of correction is to introduce an asymmetry in the difference in polar angles between the two arms of LumiCal [28].

The second consequence of the beam-beam interaction is loss of energy due to beamstrahlung. This effect causes the energy of the scattered particles to change, either before or after the Bhabha scattering. As a result, it might be required to modify the relative energy cut. In any case, it should be noted that the energy loss effect is not likely to present a problem. As will be shown below, the relative energy cut may be made rather loose, and so the changes will tend to cancel out.

In the following study, as a first approximation, we do not take the systematics from beam-beam interactions into account. Accordingly, the polar and relative energy cuts are not necessary.

4.2 Fast Simulation

In order to find the optimal set of selection cuts, samples of Bhabha events and of background events were simulated.

The sample of Bhabha scattering events, $e^-e^+ \to e^-e^+$, consisted of 10^6 events, generated at $\sqrt{s} = 3$ TeV using BHWIDE. The sample contains only events in which the leptons are scattered within $44 < \theta < 153$ mrad, the physical polar angular range of LumiCal.

To simulate physics background, a sample of 10^6 four-lepton events, $e^-e^+ \to l^-l^+$, and 10^5 corresponding hadronic events, $e^-e^+ \to q^-q^+$, have been generated with WHIZARD, with respective total cross-sections of $16.2 \cdot 10^4$ and $3.4 \cdot 10^4$ fb. The samples were simulated assuming event generation through contributions of all neutral current tree-level processes. The simulation was performed in the full polar angular range, assuming that the invariant mass of the outgoing lepton pair and that the momentum transfer of the exchanged photon are both greater

than 1 GeV [28]. .

WHIZARD is a program, which is commonly used for the calculation of multi-particle scattering cross-sections and event samples. Other physics generators, such as BDK [29], have also been used for simulating four-lepton events. While the shapes of the event distributions from different generators are compatible, the values of the cross-sections seem to vary by up to an order of magnitude [30]. Currently it is not clear which generator produces the best results. Comparison studies are planned.

As discussed above, in the current study the luminosity spectrum, due to the emission of beamstrahlung radiation, was not taken into account when generating the BHWIDE and the WHIZARD event samples. The nominal center-of-mass energy, $\sqrt{s} = 3$ TeV, was used instead.

A full simulation of the development of showers due to the Bhabha and background particles in LumiCal was not performed. Instead, a fast simulation was used. The outline of the algorithm used in the study is as follows.

1. Each class of events, $e^-e^+ \to e^-e^+$, $e^-e^+ \to e^-e^+l^-l^+$ and $e^-e^+ \to e^-e^+q^-q^+$, was treated separately.
2. For a given event, the polar angle was computed for each particle. Particles whose polar angle was outside the fiducial volume of LumiCal were discarded.
3. The four vectors of all particles which passed the fiducial cut in each direction were summed. The integrated four vector gave the energy and polar angle of the "clustered shower" in the respective direction.
4. The energy and polar angle of the "clustered shower" in the two directions was compared by computing Eqs. (15) and (16). The selection cuts (Eq. (17)) were then applied.
5. The number of background events which passed the selection cuts in each event group was rescaled to comply with the luminosity with which the Bhabha scattering sample was generated.
6. The parameters $\mathcal{E}_{cut}$ and $(B/S)_{cut}$ were computed.
7. Steps (2) - (6) were repeated for different values of the cut parameters, $\mathcal{C}_\theta$ and $\mathcal{C}_E$.

The results of the study are shown in Fig. 21. The two figures show $\mathcal{E}_{cut}$ and $(B/S)_{cut}$ as a function of the polar angle cut, $\mathcal{C}_\theta$, for several values of the relative energy cut, $\mathcal{C}_E$.

While $(B/S)_{cut}$ rises steadily with $\mathcal{C}_\theta$, the increase in efficiency levels off at high values of the polar angle cut; beyond $\mathcal{C}_\theta = 7$ mrad the increase in $\mathcal{E}_{cut}$ is small. As for the relative energy cut, a sharp increase in $\mathcal{E}_{cut}$ is apparent between $\mathcal{C}_E = 1$ and 5 %, but no significant improvement is seen for higher values of $\mathcal{C}_E$. The signal to noise ratio does increase, though, for higher $\mathcal{C}_E$ values. We therefore conclude that a reasonable set of cuts is

$$\frac{\Delta E_{r,l}}{E_{r,l}} \leq 5\% \qquad |\theta_r - \theta_l| \leq 7 \text{ mrad}, \tag{19}$$

for which

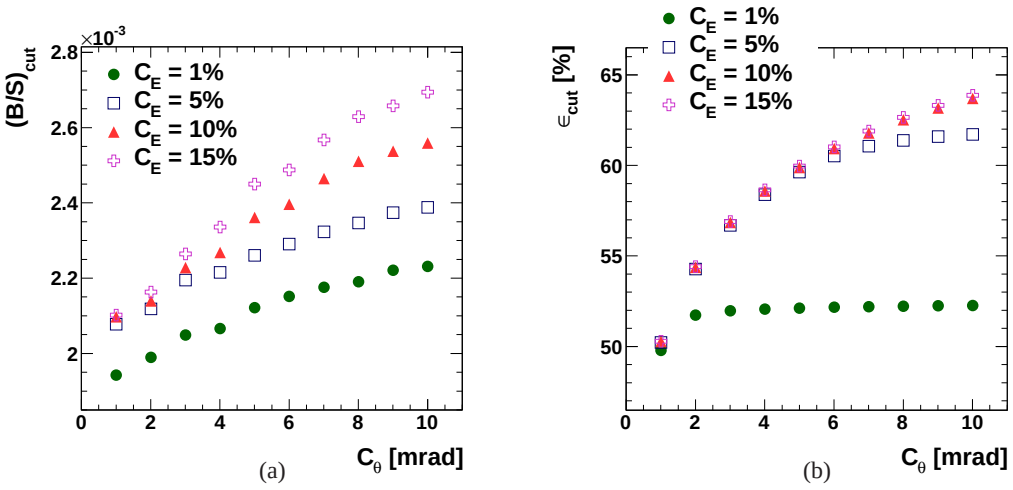

Figure 21: Background to signal ratio of the selection of Bhabha events, $(B/S)_{cut}$, (a) and the Bhabha selection efficiency, $\mathcal{E}_{cut}$, (b) as a function of the polar angle cut, $\mathcal{C}_\theta$. Different data sets are shown, corresponding to several values of the relative energy cut, $\mathcal{C}_E$, as indicated in the figures.

$$(B/S)_{cut} = 2.3 \cdot 10^{-3} \qquad \mathcal{E}_{cut} = 61\ \%. \tag{20}$$

In principle one may predict the number of background events which pass the selection cuts, $N_{bkg}(cut)$, as done above. In this case the uncertainty on the luminosity measurement depends on δN_{bkg}, the error in estimating $N_{bkg}(cut)$. One then replaces N_{rec} by $\left(N_{gen} + \delta N_{bkg}\right)$ in Eq. (2) so that together with Eq. (3)

$$\frac{\Delta\mathcal{L}}{\mathcal{L}} = \frac{\delta N_{bkg}}{N_{gen}}\Bigg|_{\theta^f_{min}}^{\theta^f_{max}}. \tag{21}$$

In light of this result, it becomes obvious that $N_{bkg}(cut)$ reflect an upper bound on the number δN_{bkg}. With this in mind, we can consider a worst-case scenario where $\delta N_{bkg} = N_{bkg}(cut)$. The bias in the luminosity measurement is then exactly the value of $(B/S)_{cut}$, which is an order of magnitude smaller than required by the design specifications of LumiCal. It should be noted that a more detailed study, in which beam-beam background, physics background and Bhabha events are overlaid, still needs to be performed.

5 Summary

The luminosity at CLIC may be measured by counting the number of Bhabha scattering events in a well defined polar angular range. In order to ensure that the cross-section is integrated in the correct polar range, the polar angle of incident showers on the luminosity calorimeter must be measurable with high precision. It has been shown here that for the proposed design of LumiCal, such a measurement is possible.

The geometry of LumiCal has been optimized, such that the polar resolution meets the precision requirements for the luminosity measurement. The energy resolution for this design was found to be roughly $0.21\ \sqrt{\text{GeV}}$. Additionally, the range of signal for the electronics readout of LumiCal was defined. Further studies on this issue ill be necessary, once it is determined whether or not MIP signals need to be read out in congruence with high-energy showers.

The issue of the background of incoherent pairs in LumiCal has been investigated in detail. It has been demonstrated that the geometric parameter which determines the influence of the beam background on the design of the calorimeter is the inner radius of LumiCal, R_{min}. For low inner radii the amount of energy which is deposited in LumiCal, as well as the number of particles which are backscattered from LumiCal, are high. For the baseline value of R_{min}, it was shown that both effects are relatively small.

Concerning the energy deposits of the incoherent pairs in LumiCal, the results depend on the number of bunch-crossings which are simultaneously read out. Provided that no more than 10 BX are read out at once, the deposited energy in LumiCal is smaller by an order of magnitude than the signal of high energy electron showers for the baseline value of R_{min}. However, if it turns out that an entire bunch-train must be integrated over, then the background-to-signal ratio of the incoherent pairs may become too large. In order to improve the ratio, topological cuts may be devised. Further study of this issue is necessary. In addition, it should be stressed that the present analysis is based on perfect head-on collisions of the CLIC bunches. Fluctuations in position and angle will change the magnitude of the beam-beam effect and of the consequent background. Further detailed studies are required.

As for the amount of backscattering from the front face of LumiCal, backscattering is greatly reduced for the baseline value of R_{min} compared to the respective cases with lower values of the inner radius. Whether or not this amount of backscattering is acceptable has not been determined. A full simulation of the entire detector is needed, and was beyond the scope of this study.

In order to distinguish Bhabha scattering events from the physics background, a set of selection cuts has been devised. It has been shown that these cuts allow a measurement of roughly 60 % of the Bhabha cross-section in the fiducial volume. The respective background-to-signal ratio is then smaller by an order of magnitude than the design goal. Further study is necessary in order to investigate the influence of the beam-beam interactions on the selection cuts. A comparative study with different physics generators is planned as well. It has further been shown that the integrated cross-section in the fiducial range of LumiCal is large, even when taking into

account a pessimistic acceptance rate of 50 %; the statistical uncertainty in counting the number of Bhabha events in this case is still smaller than the design goal. We therefore finally conclude, that it may be possible to measure the luminosity with a relative uncertainty which is smaller than 1 %.

Acknowledgments

This work is partly supported by the Commission of the European Communities under the 6th Framework Programme "Structuring the European Research Area", contract number RII3-026126, and by the Israeli Science Foundation. We would like to thank W. Lohmann for his helpful comments and suggestions. We would also like to express our appreciation of the hospitality and support given by L. Linssen, W. D. Schlatter and the other members of the Linear Collider Detector group at CERN.

References

[1] T. Becher and K. Melnikov. Two-loop QED corrections to Bhabha scattering. *JHEP 0706 084. 25 (2007)*. Also: arXiv:hep-ph/0704.3582.

[2] S. Actis, M. Czakon, J. Gluza and T. Riemann. Two-loop fermionic corrections to massive Bhabha scattering. *Nucl.Phys. B786 26-51 (2007)*. Also: arXiv:hep-ph/0704.2400.

[3] A. A. Penin. Two-loop photonic corrections to massive Bhabha scattering. *Nucl. Phys. B 734, 185 (2006)*. Also: arXiv:hep-ph/0508127.

[4] M. Czakon, J. Gluza and T. Riemann. The planar four-point master integrals for massive two-loop Bhabha scattering. *Nucl. Phys. B 751, 1 (2006)*. Also: arXiv:hep-ph/0604101.

[5] S. Jadach. Theoretical error of the luminosity cross section at LEP. *arXiv:hep-ph/0306083*, 2003. URL: http://arxiv.org/abs/hep-ph/0306083.

[6] H. Abramowicz *et al.* A Luminosity Detector for the International Linear Collider. *LC-DET-2007-006*, 2007. URL: http://www-flc.desy.de/lcnotes/notes/LC-DET-2007-006.pdf.

[7] I. Sadeh. Luminosity Measurement at the International Linear Collider, 2008. URL: http://alzt.tau.ac.il/~sadeh/mscThesis/iftachSadeh_mscThesis.pdf.

[8] H. Braun *et al.* CLIC 2008 Parameters. *oai:cds.cern.ch:1132079*, 2008. URL: http://clic-study.web.cern.ch/clic-study/.

[9] H. Abramowicz *et al.* Redefinition of the Geometry of the Luminosity Calorimeter. *EUDET-Memo-2008-09*, 2008. URL: http://www.eudet.org.

[10] MOKKA - a detailed GEANT4 detector simulation for the Future Linear Collider. URL: http://polywww.in2p3.fr/geant4/tesla/www/mokka/mokka.html.

[11] J. Allison *et al.* GEANT4 developments and applications. *IEEE Transactions on Nuclear Science 53, No. 1, 270 (2006).*

[12] MARLIN - a C++ software framework for ILC software. URL: http://ilcsoft.desy.de/portal/software_packages/marlin/index_eng.html.

[13] D. Schulte. *Ph.D. thesis, University of Hamburg*, 1996. Also: Report No. TESLA-97-08.

[14] D. Schulte. Private communication.

[15] S. Jadach, W. Placzek and B. F. L. Ward. BHWIDE 1.00: O(alpha) YFS exponentiated Monte Carlo for Bhabha scattering at wide angles for LEP1/SLC and LEP2. *Phys. Lett. B390, 298 (1997).* URL: http://arxiv.org/pdf/hep-ph/9608412.

[16] W. Kilian, T. Ohl, J. Reuter. WHIZARD: Simulating Multi-Particle Processes at LHC and ILC. *arXiv:hep-ph/0708.4233*, 2007.

[17] W. Kilian. WHIZARD Manual 1.0. *LC-TOOL-2001-039*, 2001. URL: http://www-flc.desy.de/lcnotes/.

[18] M. Moretti, T. Ohl, J. Reuter. O'Mega: An Optimizing matrix element generator. *LC-TOOL-2001-040-rev*, 2001. Also: arXiv:hep-ph/0102195. URL: http://www-flc.desy.de/lcnotes/.

[19] C. Amsler *et al.* (Particle Data Group). Review of Particle Physics. *Physics Letters B667, 1 (2008) and 2009 partial update for the 2010 edition.* URL: http://pdg.lbl.gov.

[20] T. C. Awes *et al.* A simple method of shower localization and identification in laterally segmented calorimeters. *Nucl. Inst. Meth. A311, 130 (1992).*

[21] R. Ingbir. A Luminosity Detector for the International Linear Collider, 2006. URL: http://alzt.tau.ac.il/~ronen/.

[22] H. Abramowicz *et al.* Revised Requirements on the Readout of the Luminosity Calorimeter. *EUDET-Memo-2008-08*, 2008. URL: http://www.eudet.org.

[23] H. Abramowicz *et al.* A Clustering Algorithm for the Luminosity Calorimeter. *LC-PHSM-2008-006*, 2008. URL: http://www-flc.desy.de/lcnotes/.

[24] M. Caffo *et al.* Bhabha Scattering. *Z Physics at LEP1, CERN Report 89-08, 1 (1989).* URL: http://documents.cern.ch/cgi-bin/setlink?base=cernrep&categ=Yellow_Report&id=89-08_v1.

[25] K. Mönig. Measurement of the Differential Luminosity using Bhabha events in the Forward-Tracking region at TESLA. *LC-PHSM-2000-60-TESLA*, 2000. URL: http://www-flc.desy.de/lcnotes/.

[26] B. Dalena. CLIC at 3 TeV. Talk given at the 2009 CERN FCAL meeting, URL: http://www-zeuthen.desy.de/ILC/fcal/.

[27] A. Stahl. Luminosity Measurement via Bhabha Scattering: Precision Requirements for the Luminosity Calorimeter. *LC-DET-2005-004*, 2005. URL: http://www-flc.desy.de/lcnotes/notes/LC-DET-2005-004.ps.gz.

[28] I. Smiljanic, I. Bozovic - Jelisavcic, M. Pandurovic, M. Mudrinic, J. Mamuzic. Towards a final selection for luminosity measurement. *Proceedings of the Workshop of the Collaboration on Forward Calorimetry at the ILC (Belgrade 2008), pp 52. ISBN: 978-86-7306-095-8*, 2008. URL: http://www.vinca.rs/hep/pub/FCAL_Belgrade.pdf.

[29] F. A. Berends, P. H. Daverveldt and R. Kleiss. Monte Carlo simulation of two-photon processes : I: Radiative corrections to multiperipheral $e^+e^-\mu^+\mu^-$ production. *Computer Physics Communications, Volume 40, Issues 2-3, page 271 (1986)*, 2008. URL: http://dx.doi.org/10.1016/0010-4655(86)90114-1.

[30] I. Bozovic-Jelisavcic. Background for luminosity measurement. Talk given at the June 2009 Zeuthen FCAL meeting, URL: http://www-zeuthen.desy.de/ILC/fcal/.